J. Fluid Mech. (2007), *vol.* 585, *pp.* 127–152.
doi:10.1017/S0022112007006581 Printed in the United Kingdom

Creeping motion of a sphere along the axis of a closed axisymmetric container

N. LECOQ[1], K. MASMOUDI[1], R. ANTHORE[1] AND F. FEUILLEBOIS[2]†

[1]UMR 6634 CNRS Université de Rouen, 76801 Mont Saint Aignan, France
[2]PMMH, ESPCI, 10, rue Vauquelin, 75005 Paris, France

(Received 29 January 2007 and in revised form 16 March 2007)

The creeping flow around a sphere settling along the axis of a closed axisymmetric container is obtained both theoretically and experimentally. The numerical technique for solving the Stokes equations uses the classical Sampson expansion; the boundary conditions on the sphere are satisfied exactly and those on the container walls are applied in the sense of least squares. This is an extension to the axisymmetric case of the technique for solving various two-dimensional flow problems. Two types of axisymmetric container are considered here as examples: circular cylinders closed by planes at both ends, and cones closed by a base plane. Calculated streamlines patterns show various sets of eddies, depending upon the geometry and the sphere position. Results are in agreement with earlier Stokes flow calculations of eddies in corners and in closed containers. Experiments use laser interferometry to measure the vertical displacement of a steel bead a few millimetres in diameter settling in a container filled with a very viscous silicone oil. The Reynolds number based on the sphere radius is typically of the order of 10^{-5}. The accuracy on the vertical displacement is 50 nm. Experiments show that the motion towards the apex of a cone is much slower than that towards a plane; the bead takes hours to reach the micrometre size roughness asperities on a conical wall, as compared with minutes to reach those on a plane wall. The numerical results for the drag force are in excellent agreement with experiments both for the cylindrical and the conical containers. With standard computer accuracy, the present numerical technique applies when the gap between the sphere and the nearby wall is larger than about one radius. For a sphere in the vicinity of any plane horizontal wall, these results also match with a previous analytical solution. That solution is in excellent agreement with our experimental results at small distances from the wall (typically less than a diameter, depending on the sphere size).

1. Introduction

The creeping motion of a spherical particle at a finite distance from a boundary may require a substantial correction to Stokes' law. This is because the far-field hydrodynamic interactions in Stokes flow decay slowly, as the inverse of the distance. As an example, the correction to the drag force on a sphere moving near a plane wall becomes important when the sphere–wall spacing is of the order of five diameters or less.

† Author to whom correspondence should be addressed: feuillebois@pmmh.espci.fr.

This paper is concerned with the motion of a sphere settling along the axis of an axisymmetric closed container filled with a viscous fluid, in the creeping-flow regime.

This problem may be of interest in various small-scale hydrodynamic devices in which creeping flow occurs. It also concerns the detailed flow field in a falling ball rheometer for various geometries, with the prospect of exploring the applicability of such an instrument to more complex fluids. Finally, it is the first step toward the determination of particle motion in any direction in a closed container.

In spite of the extensive literature on Stokes flow (see e.g. Happel & Brenner 1991; Kim & Karrila 1993), there appears to be little work on a particle in a closed three-dimensional container. Blake (1979) and Sano (1987) calculated the flow field generated by a Stokeslet located on the axis of a closed cylinder of finite length. Both their calculations of streamlines show the existence of a set of toroidal eddies. These eddies alternate in sign and the magnitude of the streamfunction decays exponentially with the distance from the driving singularity. However, there appear to be important differences between the calculations.

There are various numerical techniques which are appropriate to Stokes flow. The collocation technique of Ganatos, Pfeffer & Weinbaum (1980) can handle an axisymmetric system of particles. It was developed for spheres moving along the axis of an infinite cylinder or between parallel plane walls. Graham *et al.* (1989) reported some two- and three-dimensional finite-element solutions for a sphere settling in a circular cylinder. End and eccentricity effects were investigated for a number of values of the sphere to cylinder aspect ratio. The singularity technique pioneered by Youngren & Acrivos (1975) and presented in detail by Pozrikidis (1992) was also used by various authors; for example, Elasmi, Berzig & Feuillebois (2003) calculated the axisymmetric motion of a line of particles perpendicular to a plane wall. However, the case of a closed container was not studied. Another technique first developed by Bourot (1969), Coutanceau (1971) and Sigli (1970) has been used by Hellou (1988), Hellou & Coutanceau (1992), Bourot & Moreau (1987) Moreau (1988) and Moreau & Bourot (1993) to study two-dimensional Stokes flows due to motions of a cylinder in a container with a closed cross-section. Their results show various eddies which were also observed with an elaborate visualization technique by Hellou (1988). This numerical technique was *a priori* appropriate to closed containers. We therefore extend it here to three-dimensional axisymmetric flows involving a sphere moving in closed containers.

The most classical experimental way to determine the hydrodynamic interactions is to visualize the motion of a particle, e.g. a sphere, in a viscous oil. Adamczyk, Adamczyk & Van de Ven (1983) report results for the motion of a sedimenting sphere near various obstacles. Ambari, Gauthier-Manuel & Guyon (1984, 1985) imposed the displacement of a sphere with a magnetic field. They measured the force necessary to move the sphere and at the same time observed with a microscope the location of the particle.

In this paper, we use a more accurate experimental technique in which the vertical motion of a sphere is followed by Michelson laser interferometry. The typical accuracy on the measured displacement of a millimetre sized sphere is a fraction of the laser wavelength, that is, of the order of 50 nm. This technique may be used to study the hydrodynamic interactions of a vertically moving sphere with walls at various distances, in particular in the lubrication regime, as shown by Lecoq *et al.* (1993, 1995). To study the three-dimensional displacement of a sphere, this set-up was synchronized with a mechanical system following up the horizontal sphere motion (although with a lesser accuracy), (see Ekiel-Jeżewska *et al.* 1999, 2002*a*, *b*; Masmoudi *et al.* 2002).

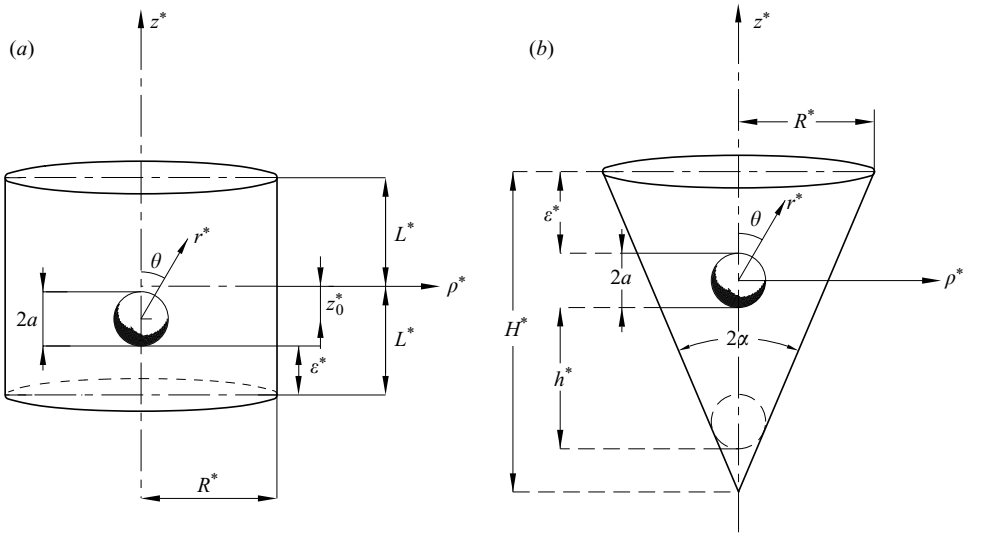

FIGURE 1. Closed containers and a moving ball. (*a*) Cylindrical container closed at both ends. (*b*) Conical container with semi-angle α closed at its top.

Although now classical, this interferometry set-up has no equivalent in providing an accurate measurement of the displacement of a sphere in the creeping-flow regime.

The specific containers studied in this article are closed cylinders and truncated cones closed by a plane wall. In all cases, the container symmetry axis is set in a vertical position. To our knowledge, there are neither comprehensive theoretical nor experimental results for these containers. Nevertheless, limited comparisons will be possible with the theoretical results for an infinite cylinder by Coutanceau (1971) and for two plane walls by Ganatos *et al.* (1980). In our calculation of streamlines, the classical works of Dean & Montagnon (1949) and Moffatt (1964) on the flow in a corner are of particular relevance to this section, since we obtain the symmetric and the antisymmetric Moffatt corner eddies. We also obtain what may be called 'interior viscous toroidal eddies' of various intensities, depending on the shape of the container and relative size of the sphere.

The outline of the paper is as follows. The basic equations for the problem and the numerical technique are described in § 2. The numerical results and comparison with other works are presented in the § 3. Various eddies obtained from the numerical calculation of streamlines are shown in § 4. The experimental set-up and procedure are described in § 5. The experimental results for the drag force and the comparison with our theoretical results and earlier ones are presented in § 6. Finally, the conclusion is in § 7.

2. Mathematical formulation and numerical procedure

Consider a spherical particle moving along the axis of an axisymmetric container. This container is either a cylinder closed at both ends or a closed conical cell pointing down. The notation is shown in figure 1. The cylinder height is $2L^*$ and that of the cone is H^*. The largest inner radius is denoted R^* in both cases. Let z^* denote a coordinate along the vertical axis of symmetry. Each container is filled with a Newtonian viscous fluid. The particle with radius a is settling along z^* in the negative

direction. Using a reference frame attached to the sphere centre, the container walls are moving with a velocity V_0 along z^*.

Normalizing all lengths with the sphere radius a, we define

$$L = L^*/a, \quad R = R^*/a, \quad z = z^*/a,$$

and so on for the various quantities displayed in figure 1. The values of the radius a, velocity V_0 and fluid kinematic viscosity ν are assumed to be such that the Reynolds number $Re = aV_0/\nu$ is low and the fluid is in creeping motion. We use V_0 and $\mu V_0/a$ as reference velocity and pressure, respectively (with μ the fluid dynamic viscosity). The fluid dimensionless velocity $\boldsymbol{v}$ and pressure p satisfy the Stokes equations. The appropriate no-slip conditions are $\boldsymbol{v} = 0$ on the sphere and $\boldsymbol{v} = \boldsymbol{e}_z$ on the container walls, where $\boldsymbol{e}_z$ denotes the unit vector along z.

The axisymmetric flow is conveniently described in term of the streamfunction Ψ, defined in spherical polar coordinates (r, θ, φ) (see figure 1) by:

$$v_r = \frac{-1}{r^2 \sin(\theta)} \frac{\partial \Psi}{\partial \theta}, \qquad v_\theta = \frac{1}{r \sin(\theta)} \frac{\partial \Psi}{\partial r}. \tag{2.1}$$

Stokes equations then give

$$\mathrm{D}^2(\mathrm{D}^2 \Psi) = 0, \tag{2.2}$$

where D^2 is the Stokesian differential operator (Happel & Brenner 1991):

$$\mathrm{D}^2 = \frac{\partial^2}{\partial r^2} + \frac{1 - \cos^2(\theta)}{r^2} \frac{\partial^2}{\partial (\cos(\theta))^2}. \tag{2.3}$$

The classical general solution of (2.2) derived by Sampson (1891) is expressed in terms of a series expansion:

$$\Psi = \sum_{n=2}^{+\infty} C_n^{-1/2}(t)(a_n r^{1-n} + b_n r^{3-n} + c_n r^n + d_n r^{n+2}), \tag{2.4}$$

where $t = \cos(\theta)$, $C_n^{-1/2}(t)$ is the Gegenbauer polynomial of degree n and order $-1/2$, and a_n, b_n, c_n and d_n are arbitrary coefficients to be determined by the boundary conditions. The terms $n = 0$ and $n = 1$ are excluded from this calculation since they would give a divergent velocity on the symmetry axis (for more details, see chap. 4 of Kim & Karrila 1993). The no-slip boundary condition on the sphere surface provides expressions for the a_n and c_n in terms of b_n and d_n. The expression (2.4) of the streamfunction then takes the form:

$$\Psi = \sum_{n=2}^{\infty} C_n^{-1/2}(t) \left[b_n \left(\frac{3-2n}{2n-1} r^{1-n} + r^{3-n} - \frac{2}{2n-1} r^n \right) + d_n \left(\frac{2}{2n-1} r^{1-n} - \frac{2n+1}{2n-1} r^n + r^{n+2} \right) \right] \tag{2.5}$$

and the components (2.1) of the fluid velocity become:

$$v_r = \sum_{n=2}^{+\infty} P_{n-1}(t) \left[b_n \left(\frac{3-2n}{2n-1} r^{-1-n} + r^{1-n} - \frac{2}{2n-1} r^{n-2} \right) + d_n \left(\frac{2}{2n-1} r^{-1-n} - \frac{2n+1}{2n-1} r^{n-2} + r^n \right) \right], \tag{2.6a}$$

	$\varepsilon = 24.00$			$\varepsilon = 11.50$			$\varepsilon = 5.25$		
N	f_{zz}^T	$\overline{\Delta V}$	$\overline{\Delta \Psi}$	f_{zz}^T	$\overline{\Delta V}$	$\overline{\Delta \Psi}$	f_{zz}^T	$\overline{\Delta V}$	$\overline{\Delta \Psi}$
15	1.09266	10^{-5}	10^{-3}	1.113	10^{-3}	10^{-2}	1.21	10^{-2}	10^{-2}
20	1.092642	10^{-6}	10^{-4}	1.1132	10^{-4}	10^{-3}	1.220	10^{-2}	10^{-2}
30	1.0926448	10^{-7}	10^{-6}	1.11321	10^{-5}	10^{-4}	1.220	10^{-3}	10^{-2}
40	1.0926448	10^{-7}	10^{-7}	1.113212	10^{-6}	10^{-5}	1.2194	10^{-3}	10^{-3}
50	1.09264480	10^{-7}	10^{-7}	1.1132174	10^{-7}	10^{-6}	1.2194	10^{-4}	10^{-3}
60	1.09264480	10^{-8}	10^{-8}	1.1132174	10^{-7}	10^{-6}	1.2193	10^{-4}	10^{-3}
70	1.09264480	10^{-8}	10^{-8}	1.1132174	10^{-8}	10^{-7}	1.2193	10^{-4}	10^{-3}

TABLE 1. Convergence of the numerical method and variations of the average residual velocity and streamfunction on the walls for a small sphere moving in a closed cylinder with normalized dimensions $L = R = 25$. In the first column, the sphere is located in the middle of the cell, in the last one, the sphere is closer to any of the plane walls.

$$v_\theta = \sum_{n=2}^{+\infty} Y_n(t) \left[b_n \left(\frac{(3-2n)(1-n)}{2n-1} r^{-1-n} + (3-n) r^{1-n} - \frac{2n}{2n-1} r^{n-2} \right) + d_n \left(\frac{2-2n}{2n-1} r^{-1-n} - \frac{(2n+1)n}{2n-1} r^{n-2} + (n+2) r^n \right) \right], \quad (2.6b)$$

where $P_n(t)$ is the Legendre polynomial of order n, and $Y_n(t) = C_n^{-1/2}(t)/s$, with $s = \sin(\theta)$. The boundary conditions on the container walls, that is $v_r = t$, $v_\theta = -s$ can be applied using the series (2.6), but they cannot be expressed in a simple way owing to the cylindrical geometry. We use instead the quadratic minimization method mentioned in § 1. The specificity here is that this method is applied to an axisymmetric flow field. The method consists in minimizing the quadratic difference between the boundary value to be imposed and the series expansions of the velocity on the container boundary:

$$J = \int_S [(v_r - t)^2 + (v_\theta + s)^2] \, \mathrm{d}S = \int_\Gamma [(v_r - t)^2 + (v_\theta + s)^2] 2\pi r s \, \mathrm{d}\Gamma \quad (2.7)$$

where Γ denotes the contour around the flow domain boundary in a meridian plane and $\mathrm{d}\Gamma$ is a line element along this contour. Since rs is bounded by R, it is sufficient to minimize:

$$I = \int_\Gamma [(v_r - t)^2 + (v_\theta + s)^2] \, \mathrm{d}\Gamma. \quad (2.8)$$

Conditions for I to be at a minimum then provide equations for the unknown coefficients b_n and d_n. For this purpose, the series (2.6) is truncated at N terms. The formulation and numerical technique are presented in the Appendix.

Estimates of the precision are obtained by calculating $\overline{\Delta V}$, average of the residual velocity $\Delta V = \sqrt{(v_r - t)^2 + (v_\theta + s)^2}$ and $\overline{\Delta \Psi}$, averaged absolute value of the residual of the streamfunction at the collocation points on the contour Γ. The maximum value accepted here for these averages is 10^{-2}. The calculation accuracy, which as expected increases with the number N of coefficients in the series, is presented in table 1 for various sphere locations in a cylinder with radius R and height $2L$, such that $R = L = 25$. The dimensionless gap between the sphere and the nearest plane wall is denoted by ε (with $\varepsilon = 0$ defined as the contact with that wall). Analogous results (not displayed here) were obtained for a sphere in a cone.

Table 1 shows that with increasing value of N, the numerical scheme converges monotically to the retained solutions to three or more significant figures for all tested spacings. Convergence is rapid and the average of the velocity deviation on the boundary decreases for increasing sphere–walls spacing. However, the technique is not appropriate when the sphere is located immediatly adjacent to the wall. The average velocity deviation then increases, owing to the presence of positive exponents in the series (2.6) which increase with distance. Details about the algorithm stability, convergence and precision are given in the Appendix.

When the sphere is close to a plane wall, we then simply use the exact solution in bispherical polar coordinates obtained by Brenner (1961) and Maude (1961) (these references are hereinafter referred to as BM). In fact, for distances to the wall of less than three radii and for $R \geqslant 3$, disturbances generated by the cylindrical or conical lateral walls can be neglected because the drag experienced by the sphere becomes large as the particle comes close to the plane wall. Fortunately, there is an overlap domain in which both calculations are in agreement (see figure 11). Now, when the sphere comes close to the vertex of the cone, no analytical solution exists, except for the lubrication solution of Masmoudi *et al.* (1998). This solution is only valid for a gap that is very small compared with the sphere radius.

Generally speaking, the convergence is better for L/R near unity and R larger than 3. It is found that the errors are greater on the upper and lower walls and that the errors on the lateral wall decay rapidly with distance. It is also found that the error on the streamfunction is largest in the corners, that is at the intersections between the endwall and the lateral wall. A similar result was obtained by Shankar (1993) who also used a least-squares method for the boundary condition on the fluid velocity. Since the fluid velocity is very low in corners, this error in Ψ does not impede the convergence of the solution; it is merely found that a comparatively larger number of terms is required to obtain the same accuracy in the vicinity of corners.

From the symmetry of the configuration and from the linearity of the Stokes equations of fluid motion, the hydrodynamic force F_z exerted upon the translating sphere may be expressed as:

$$F_z = 6\pi a \mu V_0 f_{zz}^T, \tag{2.9}$$

where the drag coefficient f_{zz}^T represents the ratio of the drag force on the sphere between walls to that on the same sphere moving with the same velocity $-V_0$ in an unbounded quiescent fluid. Coutanceau (1971) showed that:

$$F_z = 4\pi\mu a A_1 V_0 = 4\pi\mu a b_2 V_0,$$

where A_1 is the first coefficient obtained when inverting the linear system (A 2) and b_2 the first non-zero b_n coefficient in the series expansion (2.4) of the streamfunction. Equating the two expressions for the drag force yields $f_{zz}^T = (2/3)A_1$. Typical results for the drag coefficient f_{zz}^T for the sphere in a cylinder are given in table 1. The underlined numbers correspond to the last significant figure.

As an independent verification of our results, the flow field in the cylinder in the case $L = R = 25$ and $\varepsilon = 11.50$ (that is, for the sphere located in the first quarter of the cylinder) giving $f_{zz}^T = 1.1132174$ (table 1) was also calculated with the FEMLAB finite-elements package. Taking the largest mesh size on the sphere surface to be $\pi/180$ (that is, calculating the force as an integral on 180 points) provided the value $f_{zz}^T = 1.1133$. Thus, there is a 10^{-4} difference from our results. A quantitative comparison for the z-component of the fluid velocity is shown along the axis of symmetry (figure 2*a*) and

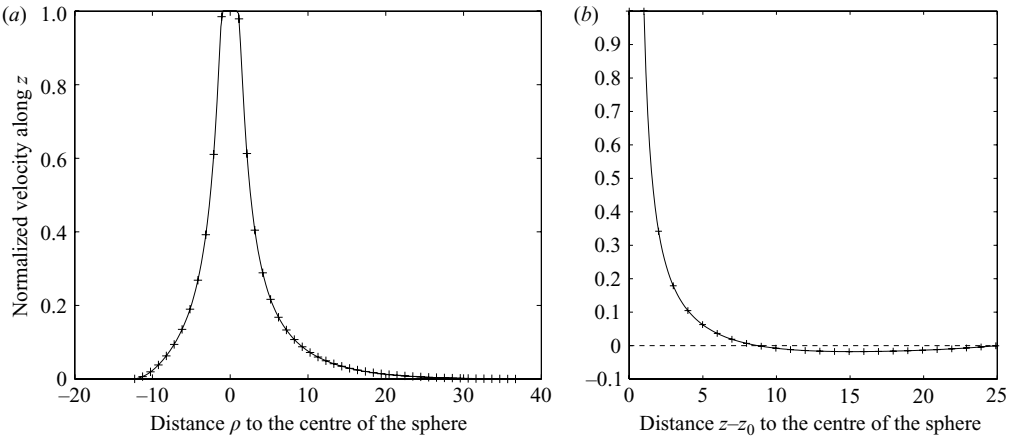

FIGURE 2. The z-component of the normalized fluid velocity around a sphere located in the first quarter of a closed cylinder with $R = 25, L/R = 1$. (*a*) Along the axis of symmetry of the cylinder. (*b*) In an equatorial plane. —, results using FEMLAB +, our calculation.

in an equatorial plane (figure 2*b*). The results are superimposed on both plots; the relative difference is of the order of 10^{-3}.

3. Results for the drag coefficient

Figure 3 shows the drag coefficient f_{zz}^T for a sphere translating along the axis of a closed cylinder for various values of R, L, ε. Results are also available as tables with the online version of the paper. For a given cylinder height $2L$, the sphere experiences the minimum drag when it is located midway between the two plane walls. The limit value obtained by Coutanceau (1971) for the drag on a sphere moving along the axis of an infinite cylinder is approached for increasing L. This condition is found in figure 3 for the middle point $(\varepsilon + 1)/(2L) = 0.5$ and for large values of L. For $R = 10$, figure 3(*b*), our result for $L = 40$ is 1.263238259 (with a 10^{-9} precision on the boundary condition on walls), whereas Coutanceau's result is 1.2629. For $R = 50$ (figure 3*c*), we find for $L = 50$ the value 1.044327198 (also with a 10^{-9} precision) and Coutanceau's result is 1.0439. That is, the limit value is approached within 10^{-3}.

The limit case of a sphere moving perpendicularly to two plane walls, which was calculated with the collocation technique by Ganatos *et al.* (1980) is also approached for large R, that is when the distance between the centre of the sphere and the plane walls is smaller than the distance between the sphere and the lateral wall of the tube. For instance, for a sphere centred midway between the plane walls: our result for $R = 50$ and $L = 6$ is 1.313 ± 10^{-3} whereas the Ganatos *et al.* (1980) result for $R \to \infty$ and $L = 6$ is 1.3265; for $R = 50$ and $L = 10$ we find 1.16873 ± 10^{-5} whereas the Ganatos *et al.* (1980) result for $R \to \infty$ and $L = 10$ is 1.1685.

The case of a semi-infinite cylinder appears in a plot for constant R (figure 3) as the limit $L \to \infty$ at constant ε (on a dashed line). It is observed that this limit is practically attained for $L \simeq 50$.

For lower values of R, the lateral wall contribution is no more negligible and the motion of the sphere is perturbed by all boundaries. For $(\varepsilon + 1)/(2L) < 0.25$, the presence of the second plane wall has no significant effect on the drag of the sphere, as demonstrated by the small slope of the curves of the isovalues of ε (dashed lines).

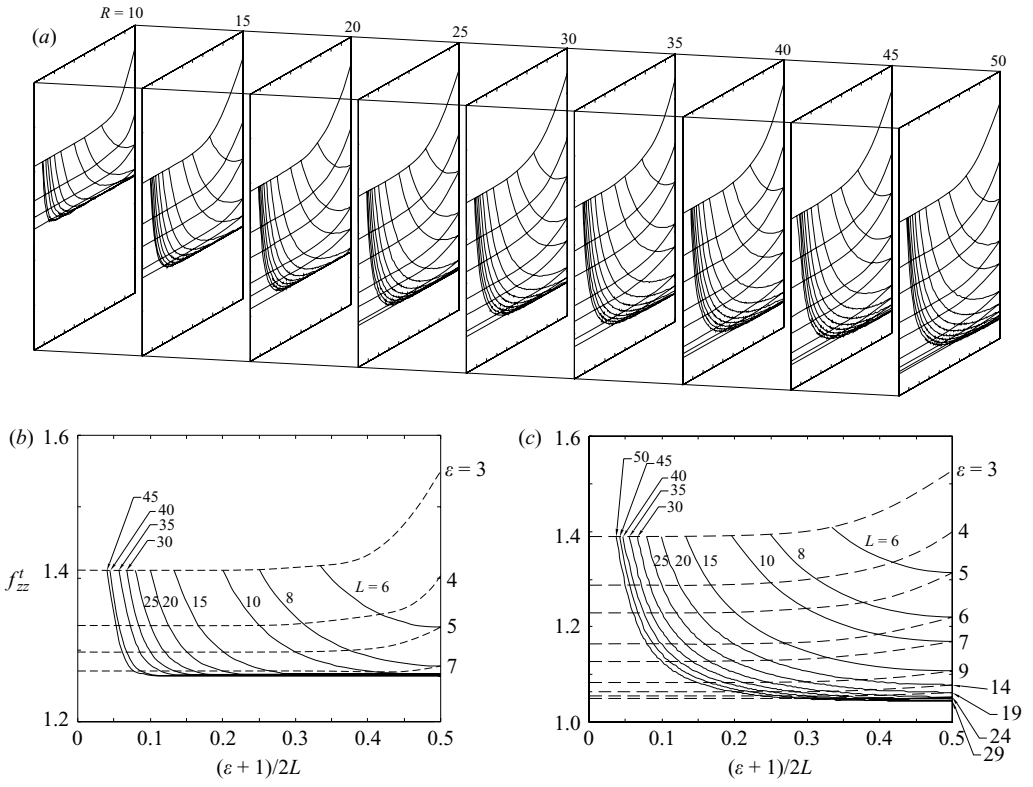

FIGURE 3. Drag coefficient for a sphere translating along the axis of a closed cylindrical container for various values of R. (*a*) Three-dimensional representation, (*b*) magnification for $R = 10$, (*c*) magnification for $R = 50$. The solid lines correspond to a constant L, and the dashed lines to a constant ε.

As discussed later, $\varepsilon = 3$ is the minimum value that can be considered with the present numerical technique.

The variation of $1/f^T_{zz}$, that is the normalized sphere velocity, is replotted in more detail in figure 4 versus the normalized position relative to the centre of the cell

$$z_0/(L-1) = 1 - \varepsilon/(L-1)$$

for the specific ratio $L/R = 0.8$ (this configuration will be used in the experiments, see §6). Our numerical results are compared to those of Sano (1987, personal communication 1990) for a small sphere moving on the axis of a closed circular cylinder. Blake (1979) presents streamlines only for several closed cylinders, and there is no possible comparison on the drag coefficient. Sano uses the assumptions $L \gg 1$, $R \gg 1$ and models the small sphere by a point-force singularity, namely, a Stokeslet. His solution is obtained as a first-order expansion in $1/L$ and $1/R$. Specifically, his result for the drag coefficient is written in the form:

$$f^T_{zz} = 1 + k^* \left(\frac{L}{R}, \frac{|z_0|}{L}\right) \frac{1}{L - |z_0|} + O\left(\frac{1}{L - |z_0|}\right)^2. \tag{3.1}$$

Sano's k^* coefficient is proportional to $\left(1/(L - |z_0|)\right)$ so that his results for $1/f^T_{zz}$ have a discontinuous derivative at $z_0 = 0$. The results of Ganatos *et al.* (1980) and

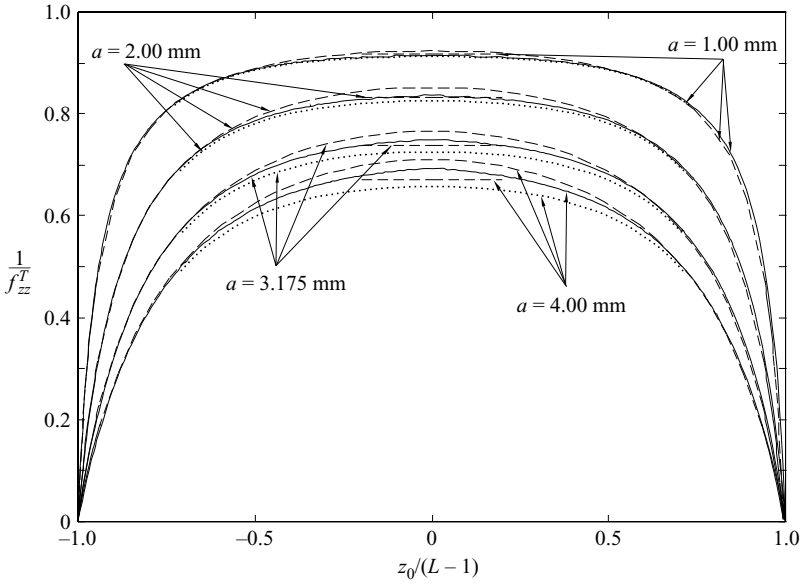

FIGURE 4. Inverse of the drag coefficient for spheres of radius a translating along the axis of a closed cylindrical container. The horizontal axis shows positions of the sphere on the axis, 1 corresponding to the top wall, -1 to the bottom wall and 0 to the midpoint (see figure 1). (Dotted lines) our numerical results for closed cylinder; (solid lines) theoretical results for a Stokeslet in a closed cylinder (Sano 1987, personal communication 1990) (curved dashed lines) theoretical value, independent of position for an infinitely long cylinder (Coutanceau 1971); (horizontal straight dashed lines) theoretical results for an infinitely wide cylinder, i.e. for a sphere falling between two infinite horizontal plates (Ganatos *et al.* 1980; Lobry & Ostrowsky 1996). $aR = 25\,\text{mm}$; $aL = 20\,\text{mm}$.

Lobry & Ostrowsky (1996) for two infinite plane walls are also shown for comparison in figure 4.

As the sphere approaches one of the plane walls, the drag becomes large and the numerical method gives a poor description of this behaviour. For $\varepsilon < 3$, we then use the exact solution obtained by BM for the motion of a sphere perpendicular to a single plane wall. For this range of ε, Lecoq *et al.* (1993) have shown that this exact solution is in excellent agreement with experiment for a sphere moving towards a plane endwall of a closed cylindrical container. For clarity, this theoretical result was not added in figure 4. The exact solution of BM matches our calculations near $\varepsilon = 2$ depending on L/R and R. For larger ε, the difference between the BM solution and the numerical calculation is due to the influence of lateral walls.

As observed in figure 4, the individual effects of the sphere volume, the lateral walls of the cylinder and the end walls combine in a non-trivial way. It is clear that a large sphere is affected by the walls of the container to a greater extent than a small sphere and that the effects of a container endwall become important only when the particle is very close to it. Our results are consistent with the boundary-element-method calculations (Graham *et al.* 1989; Tullock, Phan-Thien & Graham 1992) of the effects of lateral and endwalls experienced by a spherical particle settling in a circular container filled with a Newtonian fluid.

Consider now the results for the motion of a spherical particle settling along the axis of an infinite conical container. To our knowledge, there are no theoretical calculations of this problem, except that of Kim (1979) who used a method of

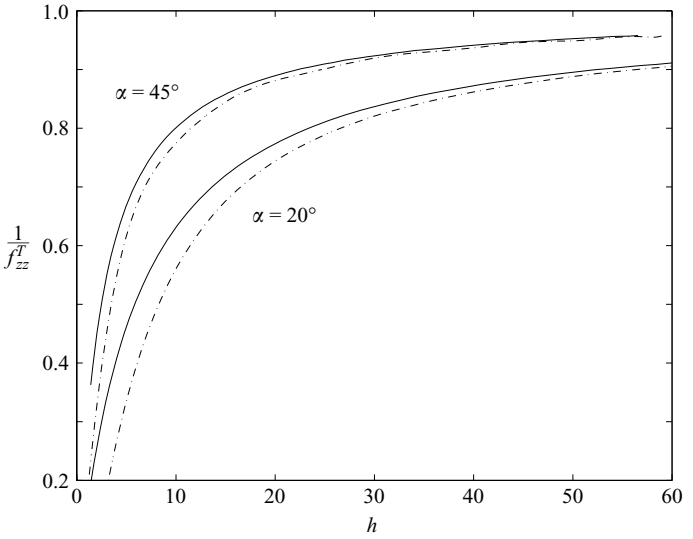

FIGURE 5. Inverse of the drag coefficient for a small sphere of radius a translating along the axis of an infinite circular cone with semi-angle at the apex $\alpha = 45°$ (top curves) and $\alpha = 20°$ (bottom curves). The horizontal axis shows the position h of the sphere on the container axis ($h = h^*/a$, see h^* in figure 1), $h = 0$ corresponds to the lowest contact position. (Dash-dotted line) our numerical results; (solid line) theoretical results for a Stokeslet (Kim 1979).

reflections to evaluate the drag experienced by a Stokeslet moving on the axis of a circular cone.

Figure 5 presents the inverse of the drag coefficient, that is the particle settling velocity normalized by its Stokes velocity in terms of $h = h^*/a$, the normalized distance to the lowest contact position (h^* is defined in figure 1). Values of $1/f_{zz}^T$ start at 0.2 since the calculation does not converge for lower values of h.

For increasing cone angle, the gap between the sphere and the lateral walls increases, so that the drag coefficient decreases. The results of Kim (1979) show that the drag coefficient is smaller for a Stokeslet than for a sphere. This is expected, since there is no volume effect for a Stokeslet. For the same reason, for increasing cone angle, our result becomes closer to that of Kim (1979) for a Stokeslet. For both angles $\alpha = 20°$ and 45°, our solution and that of Kim have the same limit behaviour when the normalized distance $h \to \infty$. This can be understood, since the volume of the particle has no effect far from boundaries.

4. Streamline patterns

The numerical procedure outlined in § 2 also provides a description of the streamline patterns. The relative normalized streamfunction Ψ is determined from (2.5) and the absolute streamfunction is then calculated as $\Psi_{abs} = \Psi + (1/2)r^2 \sin^2\theta$. In this section, we describe the shape and intensity of streamlines for several positions of the sphere. Partial comparisons with previous theoretical works are possible: (i) The flow in corners is discussed by comparison with Moffatt's antisymmetric and symmetric eddies (§ 4.1); (ii) the flow in the vertex of the cone is also compared with Wakiya's (1976) solution (§ 4.2). However, unlike Coutanceau (1971) and Hellou & Coutanceau (1992), our experimental method is not based upon the visualization of

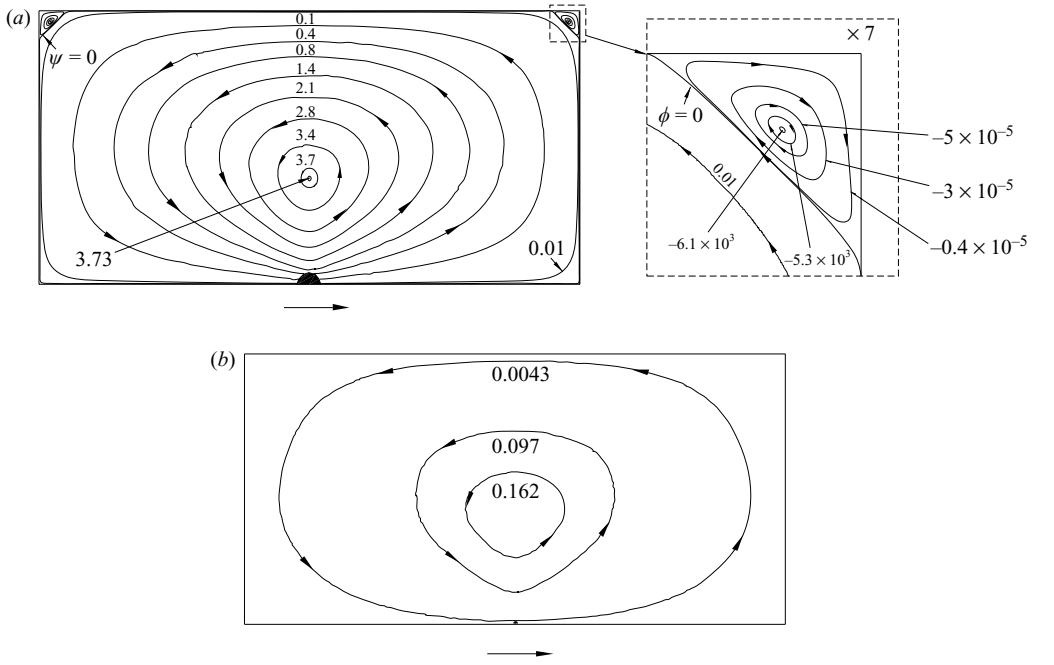

FIGURE 6. Streamlines for a sphere located in the centre of a closed cylinder with aspect ratio $L/R = 1$ and (*a*) $R = 25$. An enlargement of the corner region enclosed in a dashed square is also shown. The solution of Blake (*b*) for a Stokeslet in the centre of a closed cylinder with aspect ratio $L/R = 1$ is represented for comparison.

the flow field with solid tracers, so that comparisons with experiment cannot be made directly.

4.1. *Flow pattern in a closed cylinder*

The flow pattern for a small sphere corresponding to $R = 25$ in a closed container of aspect ratio $L/R = 1$ is presented in figure 6. The sphere is located in the centre of the cylinder. Owing to the problem axisymmetry, the flow field consists of toroidal shaped eddies, represented here in a half meridian plane. Arrows indicate the flow direction if the sphere moves conventionally to the right, as represented. The streamlines consist of a main flow (the primary eddy), that is driven directly by the particle motion, and secondary eddies in the corners. The outer streamlines of these eddies have a nearly triangular cross-section. The flow in secondary eddies is driven by the primary eddy and therefore turns in the opposite direction, as indicated also by the negative values of the streamfunction. It is observed in the enlargement that these secondary eddies are like the first of the theoretical infinite sequence of two-dimensionnal corner eddies predicted by Moffatt (1964). With our numerical precision, we could not, however, calculate beyond the secondary eddy. It is nevertheless remarkable that the ratio of intensities of the consecutive Moffatt eddies is consistent with the 10^{-5} ratio of intensities of secondary to primary eddy in our case.

Streamlines of the primary eddy are similar to those due to a Stokeslet in a closed cylindrical container, as represented by results from Blake (1979) (figure 6*b*). However, Blake's calculation does not go as far as the secondary corner eddies.

Table 2 gives a summary of the main characteristics of the primary and secondary eddies, for $R = 4$ and $L = 7.8,\ 9.5,\ 10,\ 12,\ 15$. The relevant points O, O', C and S

	$L=7.8$	$L=9.5$	$L=10$	$L=12$	$L=15$	O'Neill
$O'C$	6.85	7.14	7.14	7.14	7.14	—
OS	7.80	9.50	9.50	8.83	8.83	—
$(OS-O'C)/R$	0.2375	0.59	0.59	0.4225	0.4225	0.426
$\Psi(M_1)$	0.847	0.847	0.847	0.847	0.847	—
$\Psi(M_2)$	-3.95×10^{-6}	-1.73×10^{-5}	-2.72×10^{-5}	-4.77×10^{-5}	-5.35×10^{-5}	—
$\Psi(M_2)/\Psi(M_1)$	-4.66×10^{-6}	-2.04×10^{-5}	-3.21×10^{-5}	-5.63×10^{-5}	-6.31×10^{-5}	-7.33×10^{-5}
f_{zz}^T	1.97907078	1.97907077	1.97907077	1.979076	1.979079	—

TABLE 2. Some characteristics of the primary and secondary eddies for a sphere moving along the axis of closed cylinders with various values of the reduced semi-length L and with radius $R=4$ (see figure 7). Theoretical results of O'Neill (1983) for $L\to\infty$ are shown for comparison in the last column.

are those represented in figure 7. Note that the drag coefficient f_{zz}^T stays practically constant (up to the fifth decimal place) for varying L. This is because the primary eddy close to the sphere is practically unchanged. As evidence of this behaviour, the intensity of the primary eddy, represented here by the value of the streamfunction in the eddy centre, say $\Psi(M_1)$, is constant. On the other hand, the intensities of the secondary eddy, $|\Psi(M_2)|$, increase with L, while the eddy increases and distorts (figure 7). The outer half-length of the primary eddy, that is the distance $O'C$ (figure 7), becomes constant for $L\geqslant9.5$. On the other hand, the inner half-length of this eddy, that is the distance OS, stabilizes for $L\geqslant12$. The dividing streamline $\Psi=0$, which delineates the main driving current, detaches from the endwall at approximately $L=9.76$; then it moves towards the sphere and for $L=12$ reaches a limit position. Consequently, from this stage on, the main current becomes confined approximately to a rectangular region. In the case of an infinite cylinder, the curve $\Psi=0$ determines the quartic curve which can be used to limit the perturbed fluid domain, if secondary eddies are ignored. As remarked above, the present result is consistent with the visualization and calculation of Coutanceau (1971). From table 2, it can also be seen that the characteristic distance $(OS-O'C)/R=0.423$ for $L\geqslant12$. This value is in agreement with O'Neill (1983) who obtained $(OS(i)-O'C(i))/R=0.426$. The index (i) indicates that the result of O'Neill is valid for each of the cells in an infinite series of cells in the infinite cylinder. The next cells in the series for increasingly large L could not be calculated here because of the limitation in accuracy of our present technique. Nevertheless, this numerical technique might be extended in the manner of Moreau (1988) who calculated the analogous two-dimensional flow field due to a cylinder moving between parallel planes. The idea would be to renormalize numerical values at each cell and then match the neighbouring cells.

The previous results are still valid if the relative size of the particle is reduced. The ratio L/R determines the shape of the eddies.

Let us now consider the motion of a sphere in a squat cylinder; figure 8 presents streamlines for increasing values of R, when the sphere is located exactly in the middle of the cylinder. Toroidal secondary eddies then appear far from the sphere in the radial direction. Figures 8(a) and 8(b) show how the corner eddy pattern changes when R is increased systematically from 8 to 11.6. In the range 8 to 10.7, the corner eddy structure changes rapidly. For R close to 10.7 (and a little below), the growing corner eddies connect, leading to the formation of a continuous dividing streamline touching the middle of the lateral wall. As soon as R increases beyond 10.7, this

https://doi.org/10.1017/S0022112007006581 Published online by Cambridge University Press

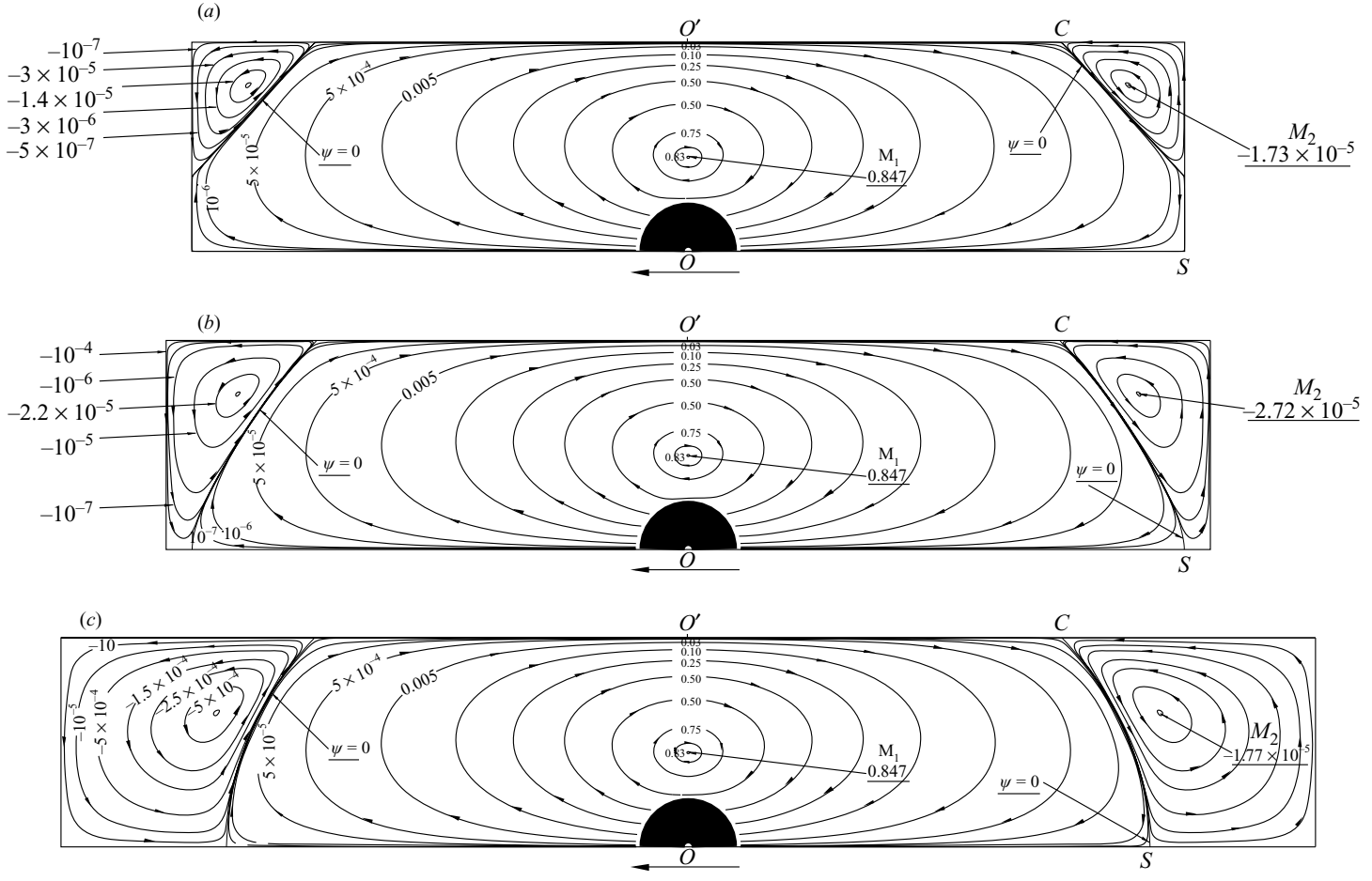

FIGURE 7. Streamlines for a sphere located in the centre of a long closed cylinder with $R=4$ and (*a*) $L=9.5$, (*b*) $L=10$, (*c*) $L=12$.

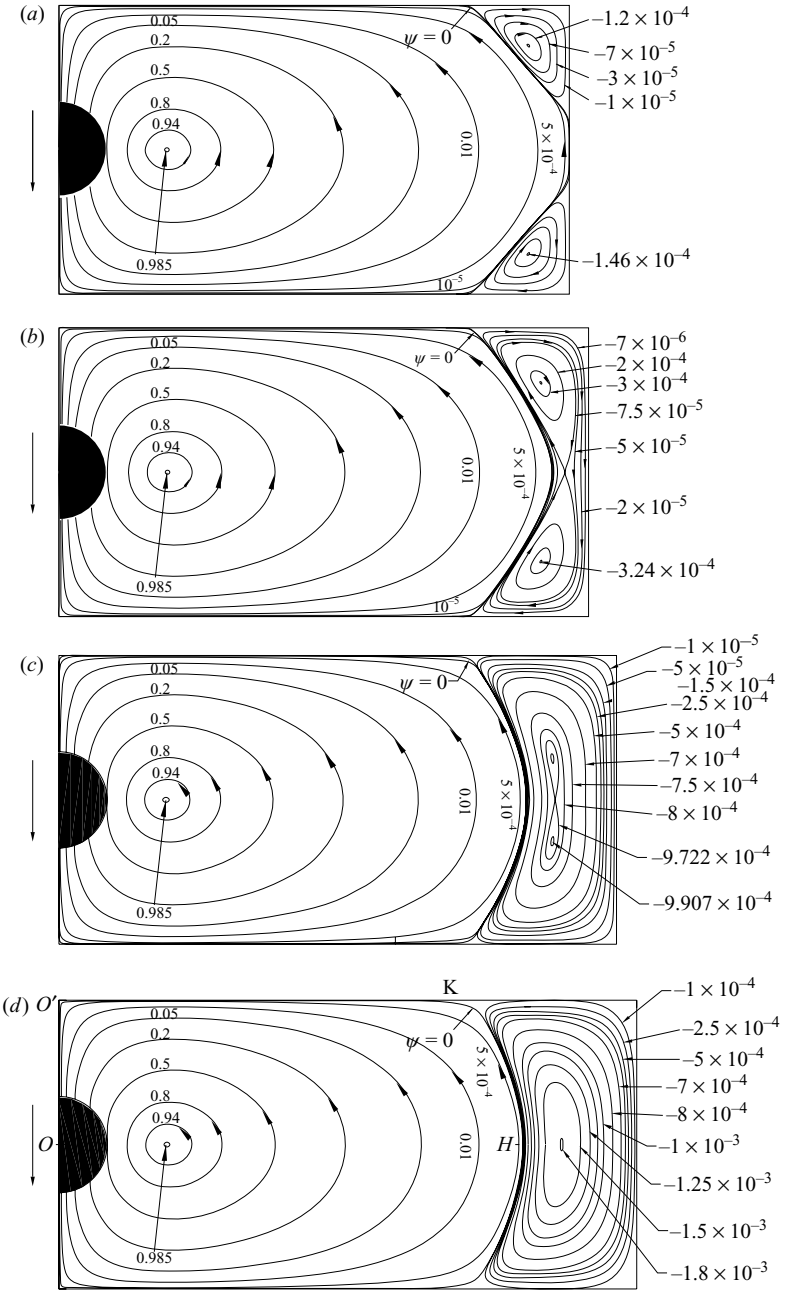

FIGURE 8. Streamlines for a sphere located in the centre of a squat closed cylinder with half-length $L = 3$ and (*a*) $R = 8$, (*b*) $R = 10.7$, (*c*) $R = 11$, (*d*) $R = 11.6$.

streamline detaches from the lateral wall and, consequently, the two corner eddies come into contact at a saddle type stationary point for Ψ (see figure 8*b*). Figures 8(*c*) and 8(*d*) show how the two corner eddies merge to produce the new secondary large eddy. The new stagnation point is located on the axis $z = 0$ owing to the symmetry of the configuration. A similar merging process was considered theoretically in detail

	$R = 10.7$	$R = 11.6$	$R = 15$	O'Neill
OH	10.6	9.625	9.366	—
$O'K$	8.49	8.49	8.49	—
$(OH - O'K)/(2L)$	0.352	0.189	0.146	0.1451
$\Psi(M_1)$	0.986	0.986	0.986	—
$\Psi(M_2)$	-1.46×10^{-4}	-3.24×10^{-4}	-1.68×10^{-4}	—
$\Psi(M_2)/\Psi(M_1)$	-1.48×10^{-4}	-3.28×10^{-4}	-1.7×10^{-3}	-2.8×10^{-3}
$\ln(\Psi(M_1)/\Psi(M_2))$	8.82	8.02	6.37	5.88
f_{zz}^T (present work)	1.8396	1.8398	1.84	—
f_{zz}^T (Lobry & Ostrowsky 1996)	1.8432	1.8432	1.8432	—

TABLE 3. Some characteristics of the primary and secondary eddies for a sphere moving along the axis of squat cylinders with various radii and with constant half-length $L = 3$ (see figure 8). The theoretical result of O'Neill for the two-dimensional flow between two parallel planes is shown for comparison. The drag coefficient f_{zz}^T obtained from our calculation is compared with the results of Lobry & Ostrowsky (1996) for two parallel planes.

by Davis *et al.* (1976 and references therein) concerning the separation from the surface of two equal spheres. Such a separation was also observed experimentally and calculated for a rotating cylinder between two parallel plane walls by Hellou & Coutanceau (1992).

For increasing R beyond $R = 11.575$, the centre of the secondary main eddy moves towards larger values of ρ and increases in strength while the line $\Psi = 0$ becomes less curved. Note that new corner eddies may appear, but as stated previously, it was not possible to calculate them with our present technique and accuracy. For larger R, beyond the value of figure 8(*d*), the secondary eddy would probably reach a limiting size and become similar to the antisymmetric eddies calculated by O'Neill (1983) and Shankar (1993) for the case of a two-dimensional flow between parallel planes. A novel eddy would then arise.

Some characteristics of the primary and secondary eddies for the squat cylinder are presented together with the result of O'Neill (1983) for two parallel planes in table 3. Let (figure 8) O be the centre of the sphere, O' the middle of the plane boundary, H and K the middle and end-points of the streamline $\Psi = 0$. The ratio $(OH - O'K)/(2L)$ decreases gradually towards the value obtained by O'Neill (1983) for the flow between parallel planes. The last row of table 3 shows the agreement between our value of the friction factor f_{zz}^T for large R and the formula obtained for two parallel planes by Lobry & Ostrowsky (1996). Note that this formula is in good agreement with the results obtained for two parallel planes by Ganatos *et al.* (1980) using the collocation method.

From this calculation, we can deduce that the secondary eddy has a very low influence on the drag coefficient.

Blake (1979), when considering a Stokeslet in the middle of a squat cylinder, obtained only a primary eddy for $L/R = 0.3$, and secondary eddies for $L/R \leqslant 0.25$ which have the same shapes as those we obtained, but are not so well defined. Sano, as in the previous cases, obtained more complicated structures.

In figure 9, the streamlines are skewed because the particle is located closer to one endwall and a large primary interior eddy occupies the whole cylinder with the exception of corners. There are two small secondary eddies in the corners, with different sizes and intensities because of the asymmetric location of the particle.

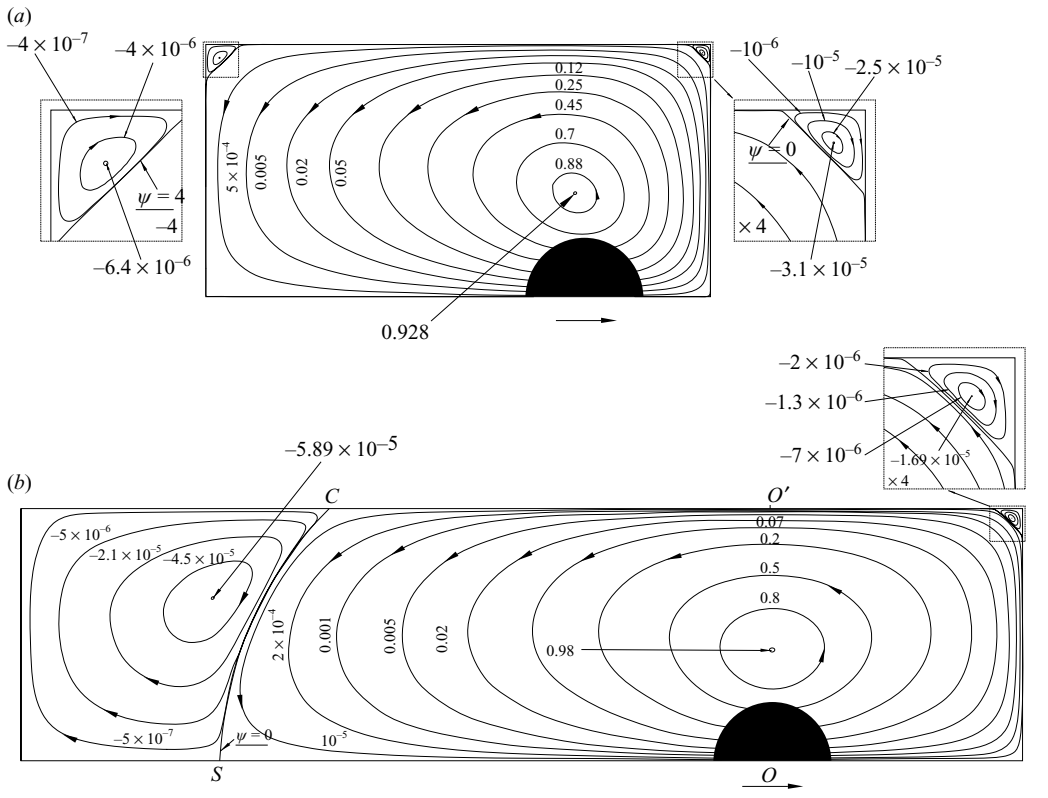

FIGURE 9. Streamlines for a sphere located in the first quarter of a closed cylinder with $R = 5$ and (*a*) $L/R = 1$, (*b*) $L/R = 2$.

Figure 9(*b*) show the existence of two large eddies (a primary and a secondary one) and the streamline $\Psi = 0$ clearly divides the cylinder into two domains.

4.2. *Flow pattern in a closed circular cone. Moffatt–Wakiya's corner eddies*

The flow patterns for closed cones with $R = 5$ and semi-angle at the apex $\alpha = 45°, 30°$ are displayed in figures 10(*a*) and 10(*b*) respectively. The sphere is located approximately in the centre of the cone. Each represented eddy is the cross-section of a vortex ring surrounding the axis of symmetry. As previously, for simplicity we have plotted only the eddies in a half meridian plane. The streamlines of the main flow (primary eddy), that is the flow directly driven by the particle in motion, are clearly obtained for both configurations. Moreover, in the top corner, there is a toroidal cell with a triangular cross section, centred on the bisecting line of the container cross-section (corner eddy). This type of eddy has been discussed in the previous section, since it corresponds to an asymmetric type of Moffatt's corner eddy. The results are summarized in table 4.

On the other hand, at the tip of the cone, two counter-rotating cells are displayed (apex eddies). The minus sign of the values of the streamfunction indicates that the secondary eddy turns in the opposite direction to the primary one. Wakiya (1976) presented the general features of a three-dimensional axisymmetric flow in a space with a conical boundary. His solution near the apex reveals features similar to Moffatt's flow. As in the two-dimensional case, Wakiya shows the existence of an

https://doi.org/10.1017/S0022112007006581 Published online by Cambridge University Press

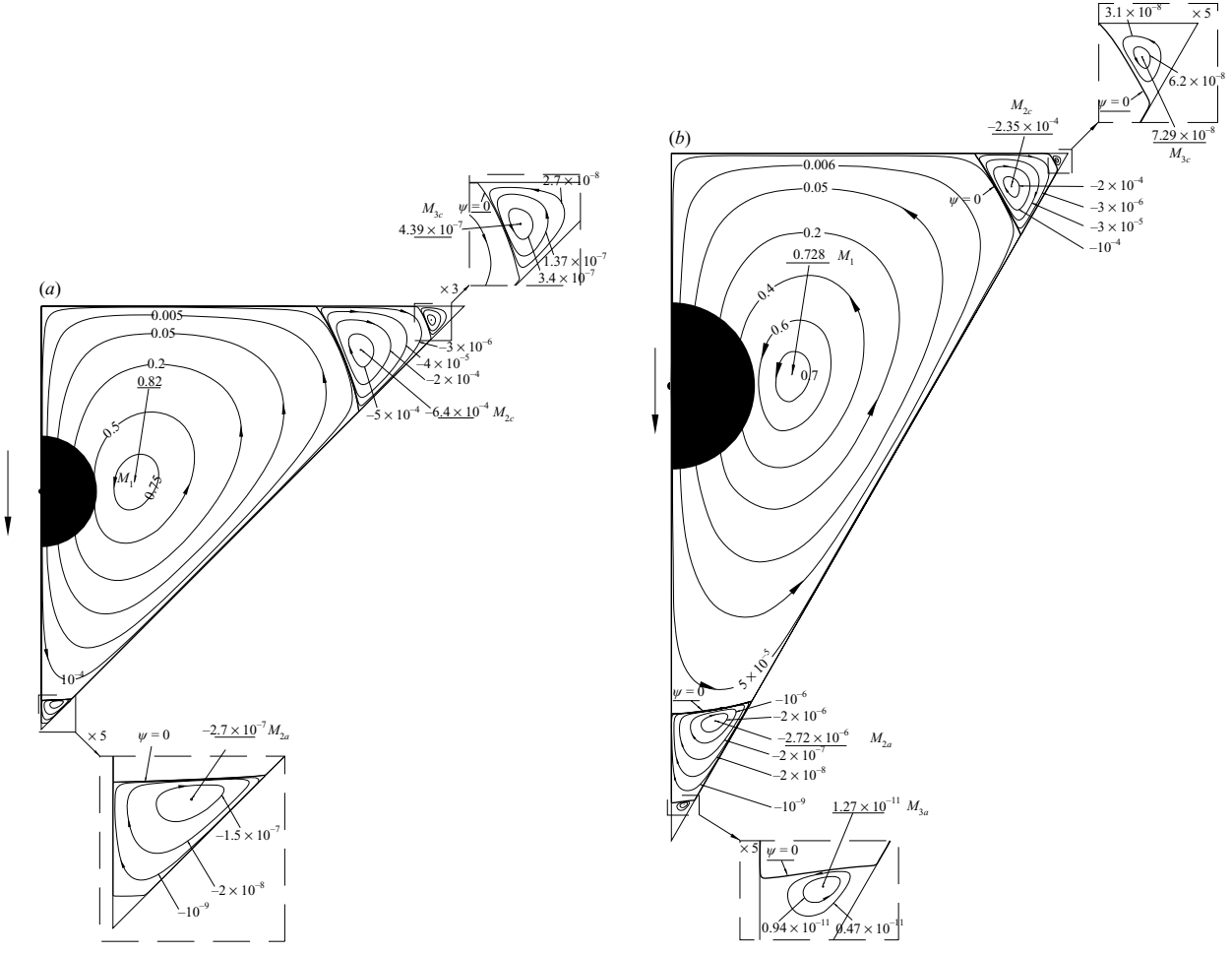

FIGURE 10. Streamlines for a sphere located in a closed cone with $R=5$ and (*a*) $\alpha=45°$, (*b*) $\alpha=30°$.

		$\alpha = 30°$			$\alpha = 45°$	
		Wakiya	Moffatt		Wakiya	Moffatt
Ψ_1	0.728	—	—	0.82	—	—
Ψ_{2a}	-2.76×10^{-6}	—	—	-2.70×10^{-7}	—	—
Ψ_{3a}	1.27×10^{-11}	—	—	—	—	—
$\ln(\Psi_1/\Psi_{2a})$	12.49	9.68	9.2	14.93	10.5	8.87
$\ln(\Psi_{2a}/\Psi_{3a})$	12.27	9.68	9.2	—	—	—
Ψ_{2c}	-2.35×10^{-4}	—	—	-6.40×10^{-4}	—	—
Ψ_{3c}	7.29×10^{-8}	—	—	4.39×10^{-7}	—	—
$\ln(\Psi_1/\Psi_{2c})$	8.04	—	6.53	7.16	—	6.15
$\ln(\Psi_{2c}/\Psi_{3c})$	8.08	—	6.53	7.28	—	6.15

TABLE 4. Some characteristics of the primary, secondary and tertiary eddies for a sphere moving along the axis of a closed cone with radius $R = 25$ and with a semi-angle at the apex equal to 30° and 45°. Index a refers to the apex eddies and c refers to the corner ones. The theoretical results of Wakiya for apex eddies and Moffatt for corner eddies are indicated for comparison.

infinite sequence of eddies near the apex. A summary of our numerical results and a comparison with Wakiya's (1976) theoretical ones is presented in table 4. In both cases of apex and corner eddies, we could calculate a tertiary one. From table 4, we observe an exponential decay in the magnitude of the streamfunction between two consecutive eddies for each case, as was predicted by Moffatt (1964) and Wakiya (1976) in the cases of corner and apex eddies, respectively.

5. Experimental set-up and measurements

The vertical displacement of a sphere along the axis of a closed container was measured with an interferometric technique. Details on the application of laser interferometry to the study of hydrodynamic interactions between a particle and walls in a viscous fluid are presented in Lecoq *et al.* (1993, 1995), and Masmoudi *et al.* (2002).

This technique is applied here to study hydrodynamic interactions between a sphere and the closed containers described above (figure 1). Spherical particles used in the experiments are steel balls manufactured by SNR with radii ranging from 1.00 to 4.00 mm. Departure from sphericity is small, typically less than 5 μm and the surface roughness observed under a scanning microscope is less than 0.5 μm. We used two cylindrical containers with inner height $2L^* = 40$ mm and diameters of $2R^* = 50$ mm and $2R^* = 80$ mm. Their lateral wall are made of Altuglas and they are closed at both ends with stuck-on windows made of a glass of optical quality. We also used two cones with the same inner height and maximal diameters as the closed cylinders. Thus their semi-angles at the apex are $\alpha = 31.6°$ and $\alpha = 45°$. The cones were made from a full cylindrical tube of Altuglas and by machining on a conical shape so that their apex is sharp and their lateral walls are smooth. Their largest inner radius is closed by a plane glass window of optical quality.

The cells contain a very viscous oil (Rhodorsyl 47V100000 manufactured by Rhône-Poulenc) with a kinematic viscosity given by the manufacturer of $\nu = 0.1$ m^2 s^{-1} at $T = 25$ °C.

The sphere is released on the container axis close to the upper horizontal wall. The accuracy in the position of the sphere relative to the axis is 20 μm (Masmoudi *et al.* 2002). The experimental set-up provides a measurement of the sphere vertical motion

versus time with an accuracy on the displacement of 50 nm. The contact position between the sphere and the wall (bottom plane wall for the cylinders or conical wall for the cones) is defined, within the experimental accuracy of 50 nm in the displacement, as that at which the particle velocity vanishes for the first time. When considering the motion toward a horizontal plane wall, this contact position is taken as the origin for the sphere-to-wall distance. The gap ε^* between the particle and the wall is defined from this origin and is therefore recalculated from the recorded displacement and from the contact position at the end of each experiment. More details on the experimental procedure can be found in Lecoq *et al.* (2004).

To obtain the drag coefficient in term of the experimentally measured particle velocity V_{exp}, we replace V_0 in (2.9) by $-V_{exp}$, and use the balance of forces on the moving sphere to show:

$$f_{zz}^T = V_{St}/V_{exp}, \tag{5.1}$$

where V_{St} is the Stokes velocity. V_{St} is calculated from the particle weight and buoyancy and from the fluid viscosity. The oil temperature is measured before and after the experiment and we take into account the variation of viscosity with temperature. During an experiment, the viscosity can change by less than 0.5%; this small variation is due to the absorption of the laser beam by the fluid and hand manipulation of the measurement cell before the experiment.

It was shown by Lecoq *et al.* (1993, 1995) that when the particle moves away from or towards a plane wall, the ratio of the measured velocity to the Stokes velocity is in excellent agreement with the theoretical result of BM. Thus, a measurement of the velocity of the particle close to the flat wall of the cell provides a way to determine the Stokes velocity. The 'experimental' Stokes velocity measured in this way was found to be in excellent agreement with the velocity calculated from the Stokes formula using the physical data given above.

6. Experimental results, comparison with calculations and discussion

Figure 11(*a*) shows that the results of the numerical calculations are superimposed onto the experimental results for values of $z_0/(L-1)$ in the intervals limited by the points T_i^j (located near ± 0.75), for the four sizes of particles and both cylinders ($i = 1, \ldots, 4$, $j = 1, 2$). The enlargement of the central dashed rectangular area, (figure 11*c*) shows the very good agreement between experiments and theoretical results for all configurations considered here. As in Lecoq *et al.* (1993), the results of Sano (1987) for the drag coefficient (not represented here) are not in good agreement with experiments even in the case of a small sphere. Figure 11(*b*) concentrates on the near-wall region. It presents the inverse of the experimental friction coefficient (dotted line), the theoretical one derived by BM (dashed line) and the results of our numerical calculation (solid line) as a function of the distance εa for the four particle sizes and the two cylinders. Close to the horizontal plane wall, the BM solution is valid in the region between contact and the vertical bars S_i^j ($i = 1, \ldots, 4$, $j = 1, 2$). The upper limits S_i^j are chosen so that the relative error between the experimental curves and the BM solution does not exceed 1%. The influence of the top wall and of the lateral boundaries then can be neglected. From the vertical bars T_i^j to the middle of the cylinder, our numerical calculation is in very good agreement with the experimental measurements. Both solutions match in the small domain $[T_i^j, S_i^j]$.

Figure 12 presents the inverse of the experimental friction coefficient (dotted lines), that determined by the numerical calculation (solid lines) and, as previously, the

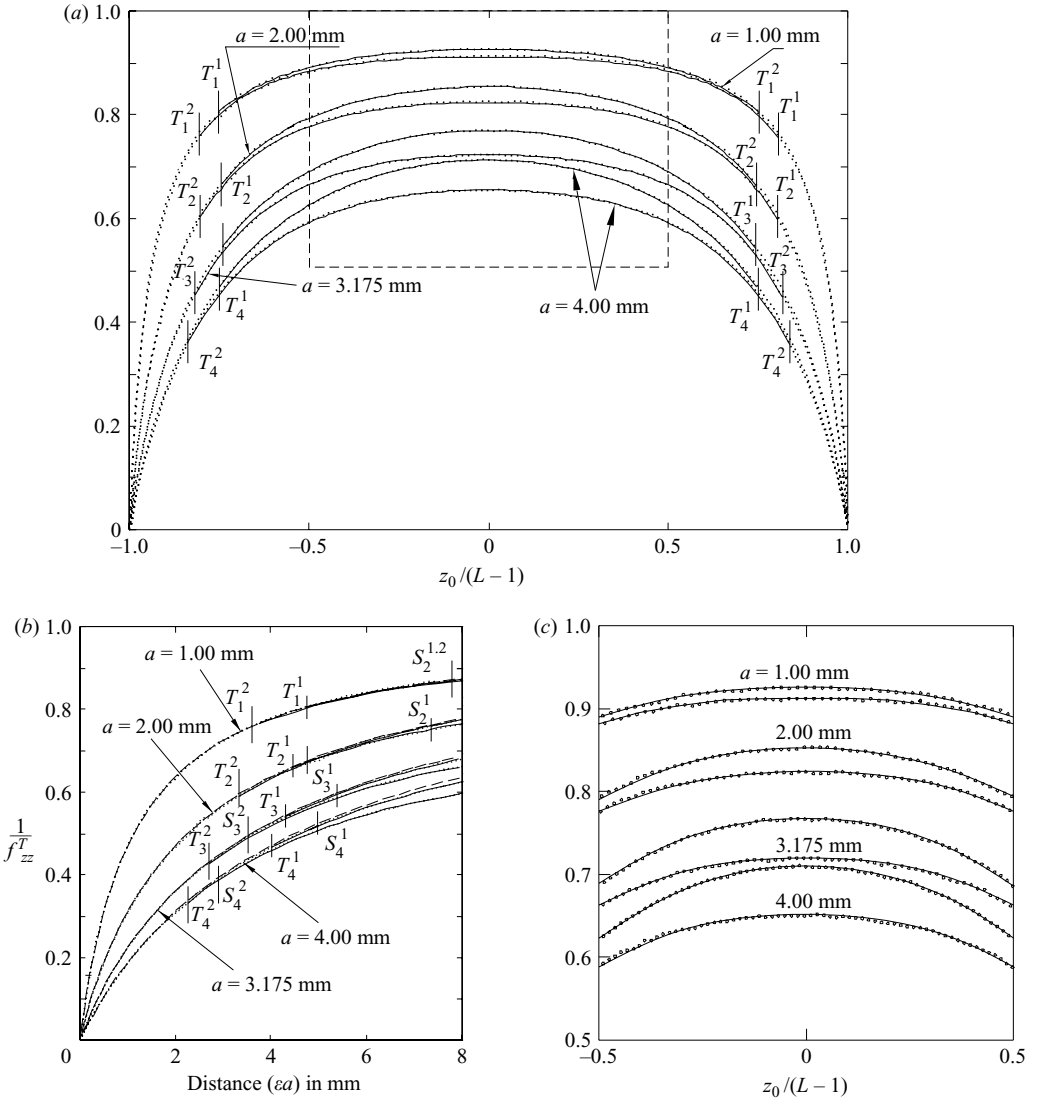

FIGURE 11. (*a*) Measured sphere normalized velocity versus normalized position relative to the centre of the cell for spheres with different radii sedimenting along the axis of closed cylindrical containers. For a given sphere, the top curve corresponds to the large cylinder. Results of our calculation (solid lines) are superimposed. The vertical bars T_i $(i = 1, \ldots, 4)$ show the limit of the calculation. The T_i^1 corresponds to the large cylinder and T_i^2 to the small one. (*b*) Enlargement of the lubrication region. The BM theoretical solution for a sphere moving towards a single plane wall (dashed lines) is superimposed on the experimental data (dotted lines). The vertical bars S_i^j $(i = 1, \ldots, 4,\ j = 1, 2)$ indicate the upper limit of the matching region between the BM solution and our calculation. (*c*) Enlargement of the dashed rectangle indicated on (*a*) showing the distribution of experimental points around the theoretical solution (solid lines).

BM solution (dashed lines) as a function of the normalized gap ξ (where $a\xi$ is the gap between the sphere and the lateral wall) for the particles with radius $a = 4.00,\ 3.175$ mm, settling along the axis of both cones. Our experimental domain being limited (ξ varies from 0 to 7.5), a comparison with the theoretical solution

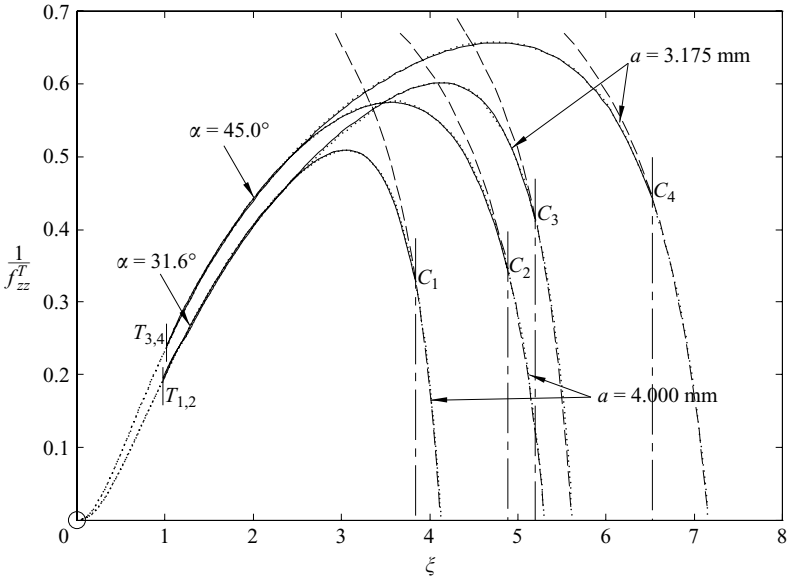

FIGURE 12. Inverse of the drag coefficient (or normalized velocity) versus normalized position for spheres with several radii settling along the axis of closed cylindrical cones: experimental results (dotted lines); theoretical results obtained with our calculation are superimposed (solid lines). The points T_i $(i = 1, \ldots, 4)$ correspond to the lower limit of the theoretical solution and the points C_i $(i = 1, \ldots, 4)$ to the upper one. The BM theoretical solution for a sphere moving towards a single plane wall (dashed lines) is superimposed on the experimental results. The circle near the origin of coordinates indicates the domain of validity of the lubrication solution obtained by Masmoudi *et al.* (1998).

proposed by Kim (1979) is not possible since that solution is valid only far from the boundaries. The results of our numerical calculation coincide with the experimental results in the domain between the vertical bars T_i $(i = 1, \ldots, 4)$ and the vertical bars C_i $(i = 1, \ldots, 4)$. The size of this domain depends on the radius of the particle and the geometry of the cone. Near the upper plane wall, the BM solution is superimposed onto the experimental results, showing that the effect of the lateral walls is negligible. As in the case of the cylinder, close to the bars C_i, there is a domain where the results of our numerical calculation match the BM solution, the difference between both sets of values being smaller than 1%. Therefore, the results of the numerical calculation completed by the BM solution allow a full determination of the velocity of the spherical particle in the upper part of a closed cone. The discrepancy between experiments and theory (least-squares method completed with BM solution) also does not exceed 1%. In the lower part of the cone, there is a gap between the present numerical solution and the lubrication solution of Masmoudi *et al.* (1998). More work is required here. Thus, apart from this region, the method of least squares is well adapted to the calculation of the drag coefficient correction of Stokes law for a sphere in motion on the vertical axis of a closed container.

7. Conclusion

The low-Reynolds-number flow driven by a spherical particle settling along the axis of symmetry of a closed container is analysed numerically and experimentally. The typical containers considered here are finite cylinders and truncated closed cones.

By adapting the least-squares method of Bourot (1969) to the axisymmetric closed geometry, the Stokes flow was calculated for various container shapes, sizes and aspect ratios. It is shown that the accuracy of the method may be carefully controlled, even though the linear system is ill-conditioned. Details are given in the Appendix. Apart from accuracy, compared with other numerical techniques an advantage of the present method is its speed. The method is appropriate provided the particle is not too close to the walls. On the other hand, the method becomes inaccurate for the treatment of lubrication phenomena since the linear system becomes too severely ill-conditioned.

Results for the flow field and drag force on the particle are provided for various values of the shape, size and aspect ratio of the container. The precision of results allows us to demonstrate special features of the complex bounded axisymmetric flow fields. These include the structure of the main eddy, the nature of the corner eddies and their eventual merging for increasing aspect ratio, leading to the formation of a new secondary eddy. Convincing comparisons are made with earlier results obtained by other authors, in particular for viscous eddies near sharp corners.

The displacement of a spherical particle settling along the axis of a closed container was measured using laser interferometry. This technique provides an accuracy of 50 nm, even for very small gaps between the particle and the wall. From this measurement, we derived the reduced velocity V_{exp}/V_{St}, that is the inverse of the friction coefficient experienced by the particle in motion. The experimental results for the friction coefficient are in excellent agreement with the theoretical solution obtained from the least-squares method, except near walls where the numerical technique loses accuracy. For a plane wall, the analytical BM solution provides the description near the wall and matches in a significant domain with our numerical solution. The numerical and experimental results show that the contributions of the volume of the sedimenting sphere, of the lateral walls of the container and of the endwall(s) combine in a non-trivial way.

This experimental technique can be used to measure hydrodynamic interactions between a particle and walls when the geometry is more cumbersome and theoretical calculations are consequently more difficult to perform. The experimental technique and numerical scheme could be applied, for instance, to a slightly deformed sphere. Finally, the flow field around a sphere near the apex of a cone and matching with the Masmoudi *et al.* (1998) lubrication solution are under consideration (see Lecoq & Feuillebois 2007).

The authors would like to thank the personnel of SCRIR at Rouen University for providing the computational facilities used for this study as well as F. Bostel (Rouen University) for his generous help in generating the streamline plots. They also thank R. Patte (Rouen University) for his advice in the tests involving several numerical methods in the final phase of the computation. The authors finally would like to thanks the referees for their valuable suggestions and comments.

Appendix. Details of the calculation and results of tests with several numerical techniques

For the computer coding, it is simpler to replace b_n and d_n by a single set of $2N$ unknown coefficients. Integrals are replaced by a summation of values at appropriately chosen collocation points.

The velocity components (2.6), with n limited to N, may be written as:

$$v_r = \sum_{j=1}^{2N} A_j F_j, \quad v_\theta = \sum_{j=1}^{2N} A_j G_j, \tag{A 1}$$

where the A_j with odd j indices correspond to the b_n and those with even j indices to the d_n. The A_j, F_j and G_j are obtained as follows.

For odd values of j, with $k = (j+1)/2 + 1$:

$$A_j = b_k,$$

$$F_j = P_{k-1}(t)\left(\frac{3-2k}{2k-1} r^{1-k} - \frac{2}{2k-1} r^{k-2}\right),$$

$$G_j = Y_k(t)\left(\frac{(2k-3)(k-1)}{2k-1} r^{-1-k} + (3-k) r^{1-k} - \frac{2k}{2k-1} r^{k-2}\right).$$

For even values of j, with $k = j/2 + 1$:

$$A_j = d_k,$$

$$F_j = P_{k-1}(t)\left(\frac{2}{2k-1} r^{-1-k} - \frac{2k+1}{2k-1} r^{k-2} + r^k\right),$$

$$G_j = Y_k(t)\left(\frac{2-2k}{2k-1} r^{-1-k} - \frac{(2k+1)k}{2k-1} r^{k-2} + (k+2) r^k\right).$$

The conditions for the integral (2.8) to be at a minimum are:

$$\frac{\partial}{\partial A_i} \int_\Gamma \left[(v_r - t)^2 + (v_\theta + s)^2\right] \mathrm{d}\Gamma = 0 \qquad (i = 1, \ldots, 2N).$$

Then, the minimization yields the linear system

$$\sum_{j=1}^{2N} A_j \int_\Gamma (F_i F_j + G_i G_j)\mathrm{d}\Gamma = -\int_\Gamma (G_i s - F_i t)\mathrm{d}\Gamma, \qquad (\mathrm{i} = 1, 2, \ldots, 2N). \tag{A 2}$$

In the system (A 2), the integrals are replaced by simple summation on an adequate number N_p of points evenly distributed along the boundary Γ: the variable of integration is the colatitude $0° < \theta < 180°$ and the points are regularly spaced with equal steps (0.5° or 0.05°). The points corresponding to $\theta = 0°$ and $\theta = 180°$ are not singular. The Gegenbauer and Legendre polynomials are obtained from a recurrence law (Press *et al.* 1990). Several methods were employed for this numerical integration: Newton–Cotes formulas and Gauss–Legendre quadrature. Results for the first 20 terms obtained with these methods were compared to the exact value obtained by analytic integration using the *Maple* computer algebra software. In every case, there is at least twelve-figures agreement between the results of the Newton–Cotes and Gauss–Legendre integrations and the exact value of the integral.

The linear system (A 2) can be written $\boldsymbol{A}\boldsymbol{x} = \boldsymbol{b}$, where $\boldsymbol{A}$ is a $2N \times 2N$, symmetric positive definite matrix and $\boldsymbol{x}$ and $\boldsymbol{b}$ are column vectors. The matrix is severely ill-conditioned; estimates of the condition number $\kappa(\boldsymbol{A})$ versus the location of the particle in the closed container and versus the number of unknowns are given in table 5. An ill-conditioned system may imply an instable solution, but this solution may still be usable, provided the residual velocity is below the required tolerance.

	$\varepsilon = 24$			$\varepsilon = 11.5$			$\varepsilon = 5.25$		
N	f_{zz}^T	$\overline{\Delta V}$	$\kappa(\boldsymbol{A})$	f_{zz}^T	$\overline{\Delta V}$	$\kappa(\boldsymbol{A})$	f_{zz}^T	$\overline{\Delta V}$	$\kappa(\boldsymbol{A})$
20	1.092642	10^{-6}	10^{64}	1.1132	10^{-4}	10^{68}	1.220	10^{-2}	10^{70}
40	1.0926448	10^{-7}	10^{125}	1.113212	10^{-6}	10^{134}	1.2194	10^{-3}	10^{138}
60	1.09264480	10^{-8}	10^{187}	1.1132174	10^{-7}	10^{199}	1.2193	10^{-4}	10^{205}
70	1.09264480	10^{-8}	10^{218}	1.1132174	10^{-8}	10^{232}	1.2193	10^{-4}	10^{239}
80	1.1	0.92	10^{248}	0.844	0.93	10^{264}	0.93	0.97	10^{272}

TABLE 5. Convergence of the numerical method and variations of the average residual velocity on the walls and condition number of the matrix $\boldsymbol{A}$ for a small sphere moving in a closed cylinder with normalized dimensions $L = R = 25$ In the first case, the sphere is located in the middle of the cell, in the last one, the sphere is closer to any of the plane walls.

This is the case here, as proved by the results presented in table 5 for $\overline{\Delta V}$, the average residual velocity on the walls. When the particle is close to the centre of the container ($\varepsilon = 24$), the condition number is very high ($\simeq 10^{64}$) for a small number of unknowns, $N = 20$. It increases up to 10^{218} for a large number of unknowns, $N = 70$, but the residual average velocity decreases to 10^{-8}. This implies that the boundary conditions are satisfied even though the linear system is severely ill-conditioned. The convergence of values of f_{zz}^T is also observed in table 5 (values are recalled from table 1). Then, for $N = 80$, $\overline{\Delta V}$ diverges strongly. There is thus an optimum number of terms in the expansion. The situation is akin to the use of non-convergent series as asymptotic expansions.

Zimmerman (2004) studied in detail series expansion solutions for creeping flows which lead to linear systems with a high condition number. He showed that this problem arises even for the simple Poisson operator. He found that the condition number increases with the order of truncation of the system and also for close surfaces. Similar situations arise in our case. Zimmerman argues that this ill-conditioning arises from an incompatibility between the shape of bounding surfaces and the natural geometry of the harmonics. Thus, if a general axisymmetric surface is to be considered, there is *a priori* no adapted type of harmonics and ill-conditioning seems to be inevitable. In spite of this drawback, precision can be controlled (Zimmerman 2004) for various series solutions and as shown here for our technique.

Several well-known direct and iterative methods were tested for solving the linear system (A 2): Gauss–Jordan and Cholesky decomposition as direct methods, Gauss–Seidel, Conjugate gradient method and MINRES (minimum residual) method as iterative procedures. The LAPACK subroutines and templates by Barrett *et al.* (1994) were used.

The Cholesky method failed rapidly because of errors during the decomposition (the matrix is severely ill-conditioned and the square roots of negative terms are computed). In a similar way, the conjugate gradient method provides good convergence only if the condition number $\kappa(\boldsymbol{A})$ of the matrix is low (lower than 100). A way to overcome the problem of a low convergence rate with a high condition number is to use a preconditioner (Axelsson 1985; Davey & Ward 2000). It is recognized that a suitable preconditioner can improve the convergence characteristics of the conjugate gradient method. Essentially, the system $K^T \boldsymbol{A} K \boldsymbol{y} = K^T \boldsymbol{b}$ is solved instead of $\boldsymbol{A}\boldsymbol{x} = \boldsymbol{b}$ where K is chosen so that $\kappa(K^T \boldsymbol{A} K) \ll \kappa(\boldsymbol{A})$. The preconditioned conjugate gradient method was applied here using several preconditioners (Jacobi, SSOR, ...). Convergence was

obtained with a limited number of iterations, but there was no significant improvement of the solution. Therefore, the linear system (A 2) was inverted using simply the Gauss–Jordan elimination method. The boundary conditions on the walls are satisfied with a ($\overline{\Delta V} \leqslant 10^{-4}$) tolerance in all considered cases.

Once the unknowns A_j of the linear system are determined, all the hydrodynamic characteristics such as the velocity and pressure fields may be calculated.

REFERENCES

Adamczyk, Z., Adamczyk, M., & Van de Ven, T. G. M. 1983 Resistance coefficient of a solid sphere approaching plane and curved boundaries. *J. Colloid Interface Sci* **96**, 204–213.

Ambari, A., Gauthier-Manuel, B. & Guyon, E. 1984 Wall effects on a sphere translating at constant velocity. *J. Fluid Mech.* **149**, 235–253.

Ambari, A., Gauthier-Manuel, B. & Guyon, E. 1985 Direct measurement of tube wall effect on the Stokes force. *Phys. Fluids* **28**(5), 156–159.

Axelsson, A. 1985 A survey of preconditioned iterative methods for linear systems of equations. *BIT* **25**, 166–187.

Barrett, R., Berry, M., Chan, T. F., Demmel, J., Donato, J., Dongarra, J., Eijkhout, V., Pozo, R., Romine, C. & Van der Vorst, H. 1994 *Templates for the Solution of Linear Systems: Building Blocks for Iterative Methods*, 2nd edn. SIAM, Philadelphia.

Blake, J. R. 1979 On the generation of viscous toroidal eddies in a cylinder. *J. Fluid Mech.* **95**, 209–222.

Bourot, J. M. 1969 Sur l'application d'une méthode de moindres carrés à la résolution approchée du problème aux limites, pour certaines catégories d'écoulements. *J. Méc. Théor. Appl.* **8**, 301–322.

Bourot, J. M. & Moreau, F. 1987 Sur l'utilisation de la série cellulaire pour le calcul d'écoulements plans de Stokes en canal indéfini: application au cas d'un cylindre circulaire en translation. *Mech. Res. Commun.* **14**(3), 187–197.

Brenner, H. 1961 The slow motion of a sphere through a viscous fluid towards a plane surface. *Chem. Engng Sci.* **16**, 242–251.

Coutanceau, M. 1971 Contribution à l'étude théorique et expérimentale de l'écoulement autour d'une sphère qui se déplace dans l'axe d'un cylindre à faible nombre de Reynolds ou en régime irrotationnel. Thèse de Doctorat d'État, Université de Poitiers.

Coutanceau, M. 1987 Confined creeping flow around an axisymmetric body: increase of the shape effect by a tube wall. *Fluid Dyn. Res.* **2**, 153–174.

Davey, K. & Ward, M. J. 2000 A successive preconditioned conjugate gradient method for the minimization of quadratic and nonlinear functions. *Appl. Numer. Maths* **35**, 129–156.

Davis, A. M. J., O'Neill, M. E., Dorrepaal, J. M. & Ranger, K. B. 1976 Separation from the surface of two equal spheres in Stokes flow. *J. Fluid Mech.* **77**, 625–644.

Dean, W. R. & Montagnon, P. E. 1949 On the steady motion of a viscous liquid in a corner. *Proc. Camb. Phil. Soc.* **45**, 389–394.

Ekiel-Jeżewska, M. L., Feuillebois, F., Lecoq, N., Masmoudi, K., Anthore, R., Bostel, F. & Wajnryb, E. 1999 Hydrodynamic interactions between two spheres at contact. *Phys. Rev.* E **59**, 3182–3191. Erratum: 1999, **60**, 4994.

Ekiel-Jeżewska, M. L., Lecoq, N., Anthore, R., Bostel, F. & Feuillebois, F. 2002*a* Rotation due to hydrodynamic interactions between two spheres at contact. *Phys. Rev.* E **66**(051504), 1–14.

Ekiel-Jeżewska, M. L., Lecoq, N., Anthore, R., Bostel, F. & Feuillebois, F. 2002*b* Interactions between two close spheres in Stokes flow. In *Tubes, Sheets and Singularities in Fluid Dynamics, Proc. IUTAM Symp. Zakopane, Poland, 2–7 September* vol. 9 of *Fluid Mechanics and its Applications* (ed. K. Bajer & H. K. Moffatt), pp. 343–348. Kluwer.

Elasmi, L., Berzig, M. & Feuillebois, F. 2003 Stokes flow for the axisymmetric motion of several spherical particles perpendicular to a plane wall. *Z. Angew. Math. Phys.* **54**, 304–327.

Ganatos, P., Pfeffer, R. & Weinbaum, S. 1980 A strong interaction theory for the creeping motion of a sphere between plane parallel boundaries. Part 1. Perpendicular motion. *J. Fluid Mech.* **99**, 739–754.

Graham, A. L., Mondy, L. A., Miller, J. D. Wagner, N. J. & Cook, W. A. 1989 Numerical simulations of eccentricity and end effects in falling ball rheometry. *J. Rheol.* **33**, 1107–1128.

Habermann, W. L. & Sayre, R. M. 1958 David Taylor model basin. Rep. 1143, Washington DC, US Navy Dept.

Happel, J. & Brenner, H. 1991 *Low Reynolds Number Hydrodynamics*, 5th edn. Kluwer.

Hellou, M. 1988 Etude numérique et expérimentale de l'écoulement à structure cellulaire, engendré par la rotation d'un cylindre dans un canal. Thèse de Doctorat, Université de Poitiers.

Hellou, M. & Coutanceau, M. 1992 Cellular Stokes flow induced by rotation of a cylinder in a closed channel. *J. Fluid Mech.* **236**, 557–577.

Kim, M. U. 1979 Slow viscous flow due to the motion of a sphere on the axis of a circular cone. *J. Phys. Soc. Japan* **47**, 1670–1675.

Kim, S. & Karrila, S. J. 1993 *Microhydrodynamics: Principles and Selected Applications.* Butterworth–Heinemann.

Lecoq, N. & Feuillebois, F. 2007 Lubrication in a flat cone: the transition from a cone to a plane wall. *Phys. Fluids* **19**, 038103.

Lecoq, N., Feuillebois, F., Anthore, N., Anthore, R. Bostel, F. & Petipas, C. 1993 Precise measurement of particle–wall hydrodynamic interactions at low Reynolds number using laser interferometry. *Phys. Fluids* A **5**(1), 3–12.

Lecoq, N., Feuillebois, F., Anthore, R., Petipas, C. & Bostel, F. 1995 Experimental investigation of the hydrodynamic interactions between a sphere and a large spherical obstacle. *J. Phys. Paris* II **5**, 323–334.

Lecoq, N., Anthore, R., Cichocki, B., Szymczak, P. & Feuillebois, F. 2004 Drag force on a sphere moving towards a corrugated wall. *J. Fluid Mech.* **513**, 247–264.

Lobry, L. & Ostrowsky, N. 1996 Diffusion of Brownian particles trapped between two walls: theory and dynamic-light-scattering measurements. *Phys. Rev.* B **53**, 12 050–12 056.

Masmoudi, K., Lecoq, N., Anthore, R., May, S. & Feuillebois, F. 1998 Lubricating motion of a sphere in a conical vessel. *Phys. Fluids* **10**(5), 1231–1233.

Masmoudi, K., Lecoq, N., Anthore, R., Bostel, F. & Feuillebois, F. 2002 Accurate measurement of hydrodynamic interactions between a particle and walls. *Exps. Fluids* **32**(1), 55–65.

Maude, A. D. 1961 End effects in falling-sphere viscometer. *Br. J. Appl. Phys.* **12**, 293–295.

Moffatt, H. K. 1964 Viscous and resistive eddies near a sharp corner. *J. Fluid Mech.* **18**, 1–17.

Moreau, F. 1988 Etude de la série cellulaire, bidimensionnelle et complexe, et de ses applications aux écoulements de Stokes en canal plan. Thèse de Doctorat, Université de Poitiers.

Moreau, F. & Bourot, J. M. 1993 Ecoulements cellulaires de Stokes produits en canal plan illimité par la rotation de deux cylindres *Z. Angew. Math. Phys.* **44**, 777–798.

O'Neill, M. E. 1983 On angles of separation in Stokes flow. *J. Fluid Mech.* **133**, 427–442.

Pozrikidis, C. 1992 *Boundary Integral and Singularity Method for Linearized Viscous Flow.* Cambridge University Press.

Press, W. H., Flannery, B. P., Teukolsky, S. A. & Vetterling, W. T. 1990 *Numerical Recipes in C, the Art of Scientific Computing.* Cambridge University Press.

Sampson, R. A. 1891 On Stokes's current function, *Phil. Trans. R. Soc.* A **182**, 449.

Sano, O. 1987 Mobility of a small sphere in a viscous fluid confined in a rigid circular cylinder of finite length. *J. Phys. Soc. Japan* **56**, 2713–2720.

Shankar, P. N. 1993 The eddy structure in Stokes flow in a cavity. *J. Fluid Mech.* **250**, 371–383.

Sigli, D. 1970 Contribution à la mise au point d'une technique de résolution approchée du problème aux limites, pour un écoulement de révolution en régime de Stokes. Thèse de 3ème Cycle, Université de Poitiers.

Tullock, D. L., Phan-Thien, N. & Graham, A. L. 1992 Boundary element simulations of spheres settling in circular, square and triangular conduits. *Rheol Acta* **31**, 139–150.

Wakiya, S. 1976 Axisymmetric flow of a viscous fluid near the vertex of a body. *J. Fluid Mech.* **78**, 737–747.

Youngren, G. K. & Acrivos, A. 1975 Stokes flow past a particle of arbitrary shape: numerical method of solution. *J. Fluid Mech.* **69**, 377–403.

Zimmerman, W. B. 2004 On the resistance of a spherical particle settling in a tube of viscous fluid. *Intl J. Engng Sci.* **42**, 1753–1778.